

1 **Interface Passivation to Overcome Shunting in Semiconductor-Catalyst** 2 **Junctions**

3 Parisa Shadabipour and Thomas W. Hamann*

4 *Department of Chemistry, Michigan State University 578 South Shaw Lane, East Lansing,*
5 *Michigan 48824-1322, United States*

6

7

8 **Experimental:**

9 Hematite thin films were prepared on Fluorine-doped tin oxide (FTO) coated
10 aluminoborosilicate glass substrate (Solaronix, 10 Ω /sq) via electrodeposition (ED) and atomic
11 layer deposition (ALD) methods using the procedure described previously.^{1,2} Before hematite
12 deposition, FTO substrates were cleaned by sequential sonication in soap, water, and isopropyl
13 alcohol for about 15 min, followed by drying in an N₂ stream. The electrodeposition of hematite
14 thin film was performed by submerging the FTO substrate in a solution of 0.1 M FeCl₂·4H₂O
15 (pH~4.3) at 60 °C by applying the constant potential of 1.2 V vs. Ag/AgCl for 30 min under gentle
16 stirring. Then, amorphous FeOOH film was converted to crystalline Fe₂O₃ by annealing at 800 °C
17 for 10 min. The thickness of the hematite film prepared with this method measured to be 25 nm
18 using atomic force microscopy (AFM).

19 Hematite film was also deposited on 2 nm Ga₂O₃ underlayer by ALD method. Ga₂O₃
20 underlayer was deposited on FTO substrate by ALD using a modified version of the previously
21 reported procedure.³ The Ga₂O₃ was deposited using tris-(dimethylamido) gallium (III)
22 (Ga₂(NMe₂)₆) (Strem Chemical Inc.) as the metal precursor and H₂O as an oxidant. During the
23 deposition of Ga₂O₃, Ga cylinder was heated to 150 °C and pulsed for 0.2 s under exposure mode
24 for 8 s, followed by a 12 s purge. In order to oxidize gallium precursor a 0.015 s pulse of H₂O was
25 then introduced under the same exposure time. Using spectroscopic ellipsometry (Horiba Jobin

26 Yvon, Smart-SE), the growth rate of $\sim 1.1 \text{ \AA} \text{ Ga}_2\text{O}_3$ per cycle was measured on silicon wafers.
27 Then $\sim 30 \text{ nm}$ hematite was deposited on Ga_2O_3 underlayer. The precursors for deposition of ALD-
28 hematite was ferrocene, and wet ozone was used as the oxidation source. During the deposition,
29 the ferrocene cylinder was heated to $70 \text{ }^\circ\text{C}$ and pulsed for 20 s , followed by purging. Then, an
30 oxidation cycle consists of 10 sub-cycles of a 0.015 s H_2O pulse followed by a 2 s ozone pulse
31 where each sub-cycle was separated by a 5 s purge. In the end, ALD- Fe_2O_3 film was annealed at
32 $500 \text{ }^\circ\text{C}$ for 2 h and followed by annealing in a preheated furnace at $800 \text{ }^\circ\text{C}$ for 4 min .

33 ***Electrodeposition of poly (phenylene oxide) (PPO):*** To block exposed FTO on ED-
34 hematite films, poly (phenylene oxide) (PPO) blocking layer, was selectively polymerized onto
35 the exposed FTO. The electropolymerization of PPO was performed according to the previous
36 report.⁴ Briefly, the ED-hematite electrodes were submerged in a solution containing 60 mM
37 phenol, 90 mM 2-allylphenol, and 100 mM LiClO_4 in 10/10/1 water/ethanol/2-butoxyethanol. The
38 solution was adjusted to $\text{pH } 9$ by the addition of 10 mM tetrabutylammonium hydroxide in
39 methanol. The potential of the electrodes was then scanned in the dark with the scan rate of 100
40 mV s^{-1} from 0.1 to 1.5 V versus Ag/AgCl for 75 cycles. In order to remove unreacted monomers
41 and oligomers, the electrode was soaked in 10 mM tetrabutylammonium hydroxide in methanol
42 for 10 min . In the end, the electrode was rinsed with ethanol, and cured in the air at $150 \text{ }^\circ\text{C}$ for 30
43 min . We measured the thickness of the PPO layer to be 12 nm using ellipsometry (Horiba Jobin
44 Yvon, Smart-SE) on a silicon wafer coated with gold subjected to the same polymerization
45 treatment as described above.

46 ***Catalyst deposition:*** $\text{Ni}_{0.75}\text{Fe}_{0.25}\text{O}_x\text{H}_y$ catalyst was deposited on 1 cm^2 of freshly prepared
47 ED-hematite photoanode through the spin coating of the metal precursor solution.⁵ Before catalyst
48 deposition, hematite films were rinsed with deionized water and dried with N_2 . Iron (III) 2-ethyl

49 hexanoate (50% w/w in mineral spirits, Strem Chemicals), and nickel (II) 2-ethyl hexanoate (78%
 50 w/w in 2-ethyl hexanoic acid, Strem Chemicals) were used as a precursor. An appropriate amount
 51 of metal precursor was dissolved in hexane to obtain a total concentration of 15% w/w metal
 52 complex, and further diluted with hexane to obtain a total metal concentration of 50 mM.
 53 Approximately 200 μ L of the precursor solution was placed on the substrate, and spinning was
 54 performed at 3000 rpm for 60 s. The as-prepared catalyst/ED-hematite photoelectrode was treated
 55 with UV light for 2 h to decompose organic residues (254 nm, 4 W) followed by annealing in a
 56 preheated furnace at 100 °C in air for 1 h. The thickness of $\text{Ni}_{0.75}\text{Fe}_{0.25}\text{O}_x\text{H}_y$ is is \sim 220 nm,
 57 determined using AFM, cross-sectional scanning electron microscopy (SEM) and spectroscopic
 58 ellipsometry (SE).

Measured thickness with AFM	Measured thickness with SE	Measured thickness with cross-sectional SEM
220 nm	210 nm	220 nm

59
 60 **Table S1. The measured and calculated thickness of the Ni75 on hematite using AFM and SEM, and**
 61 **on silicon wafer using SE.**

62
 63 ***(Photo)electrochemical measurements:*** All electrochemical and photoelectrochemical
 64 measurements were taken in a custom made photoelectrochemical cell setup with an Eco Chemie
 65 Autolab potentiostat (Nova electrochemical software) in back illumination configuration (photon
 66 passing through the glass before reaching to the electrode surface). A homemade saturated
 67 Ag/AgCl and high surface area Pt mesh were used as reference and counter electrode, respectively.
 68 All (photo) electrochemical measurements were performed at room temperature and in 1.0 M

69 KOH. Aqueous solutions were prepared with ultra-pure water (resistivity 18 MΩ.cm) from a Milli-
70 Q water purifier.

71 A 450 W Xe arc lamp (Horiba Jobin Yvon) was used as a white light source with an AM
72 1.5 solar filter to obtain a simulated solar spectrum with 100 mW cm⁻² (1 sun) intensity. All
73 electrochemical potentials vs. Ag/AgCl were converted to the reversible hydrogen electrode
74 (RHE) by using equation 1:

$$75 \quad E_{RHE} = E_{Ag/AgCl} + 0.197 \text{ V} + (0.059 \text{ V}) \times pH \quad \text{eq.1}$$

76 Ni_{0.75}Fe_{0.25}O_xH_y film was conditioned by a series of cyclic voltammograms between 0.5
77 and 1.6 V vs. RHE under illumination until Ni reduction peak remains constant. The *J-E* data
78 shown for the catalyst-modified electrodes are from the final measurement.

79 **Material characterization:** Scanning electron microscope (SEM) images were taken using
80 JEOL 7500F (field emission emitter). The cross-sectional sample for scanning transmission
81 electron micrograph (STEM) was prepared using Thermal Fisher Helios 650 Nanolab SEM/FIB.
82 Gold and platinum were deposited at the surface of the sample to protect it during the sample
83 preparation. The high-angle annular dark-field scanning transmission electron microscopy
84 (HAADF-STEM) and energy-dispersive x-ray (EDX) analysis were taken on a Thermo Fisher
85 Scientific Talos F200X operated at 200 kV. The X-ray photoelectron spectroscopy (XPS) data
86 were collected using PerkinElmer Phi 5600 ESCA system equipped with a monochromatic Mg Kα
87 source to illuminate the sample at a takeoff angle of 45°.

88

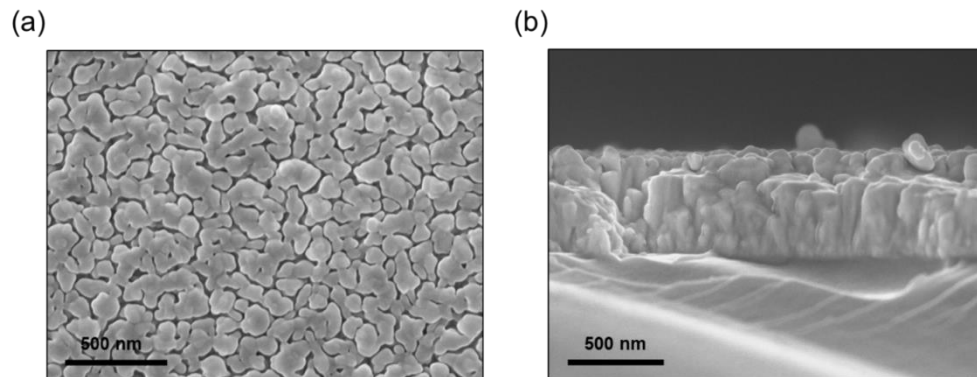
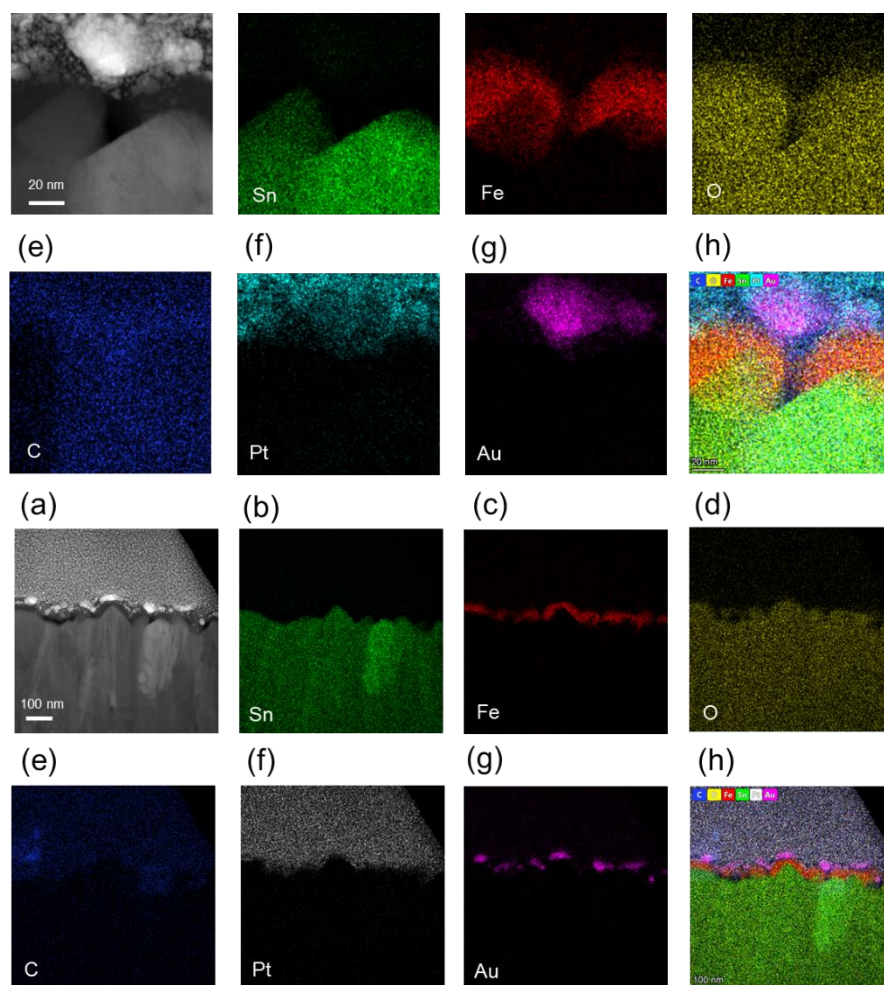
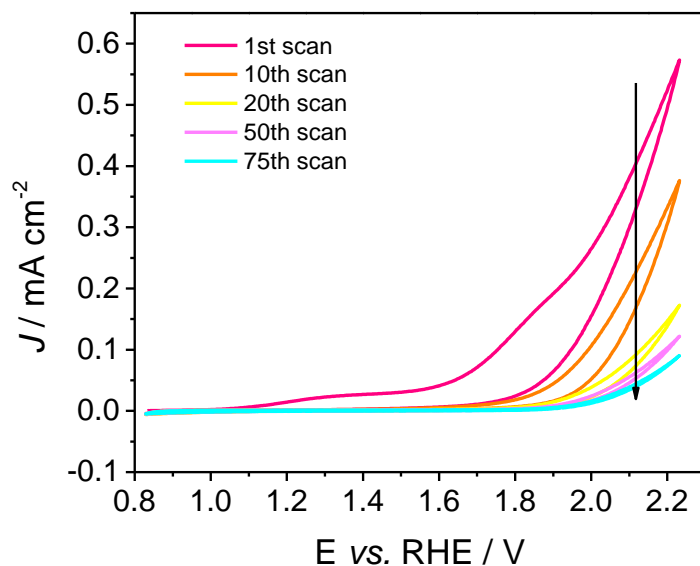


Figure S1. Scanning electron microscopy images of ED-hematite on FTO substrate. (a) top view (b) cross-sectional view



89
 90 **Figure S2. HAADF-STEM and EDX elemental mapping of the PPO-modified ED-hematite. (a)**
 91 **HAADF-STEM image and (b-h) EDX mapping of tin (b), iron (c), oxygen (d), carbon (e), platinum (f),**
 92 **gold (g) and their overlay (h).**



93 **Figure S3. Current density measurements during electrodeposition of PPO into the ED-hematite**
 94 **pinholes.** The progressive decrease in the current density indicates the growth of the insulating PPO film.
 95 Scan rates are 100 mV s^{-1} .

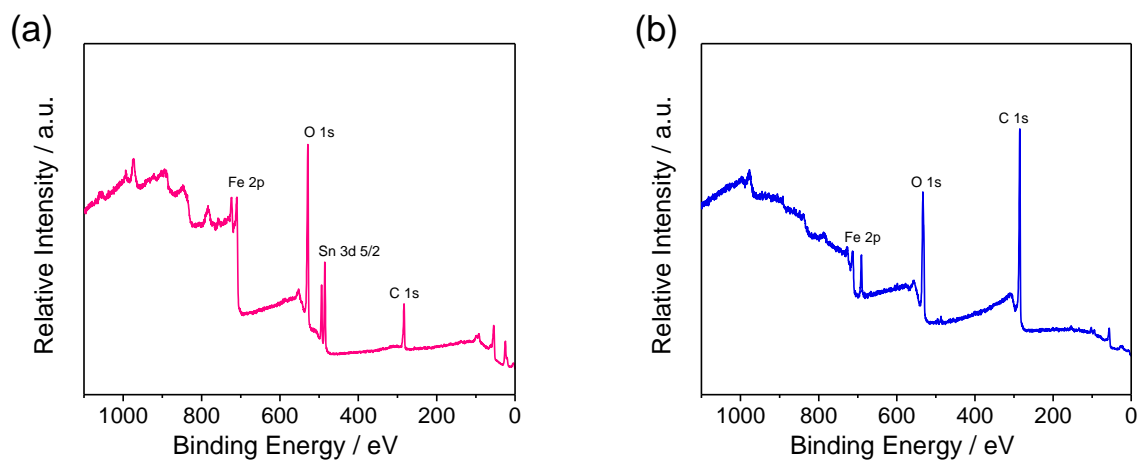
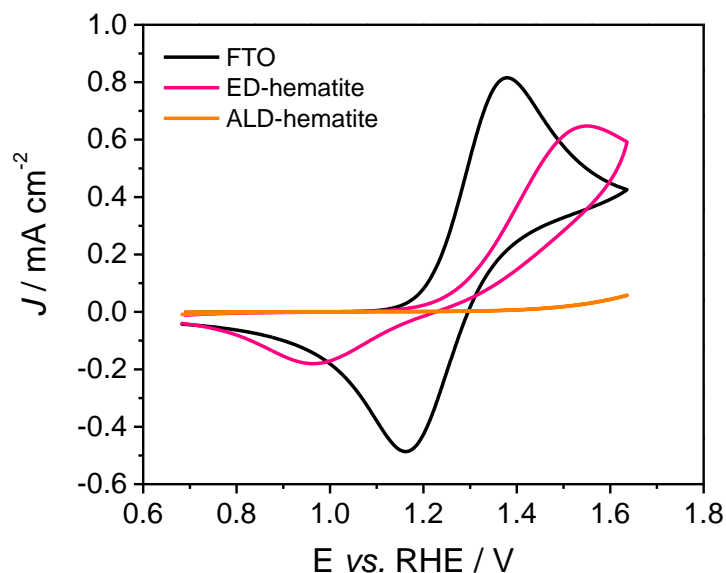


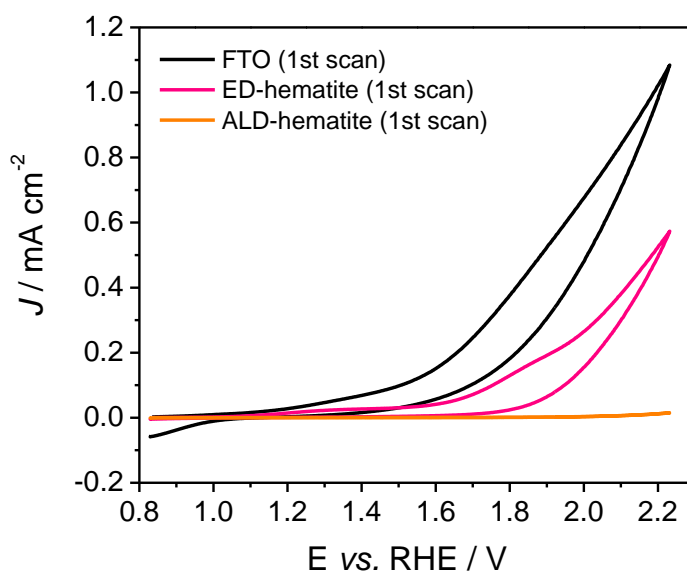
Figure S4. XPS measurement of (a) bare ED-hematite and (b) PPO modified ED-hematite.

96

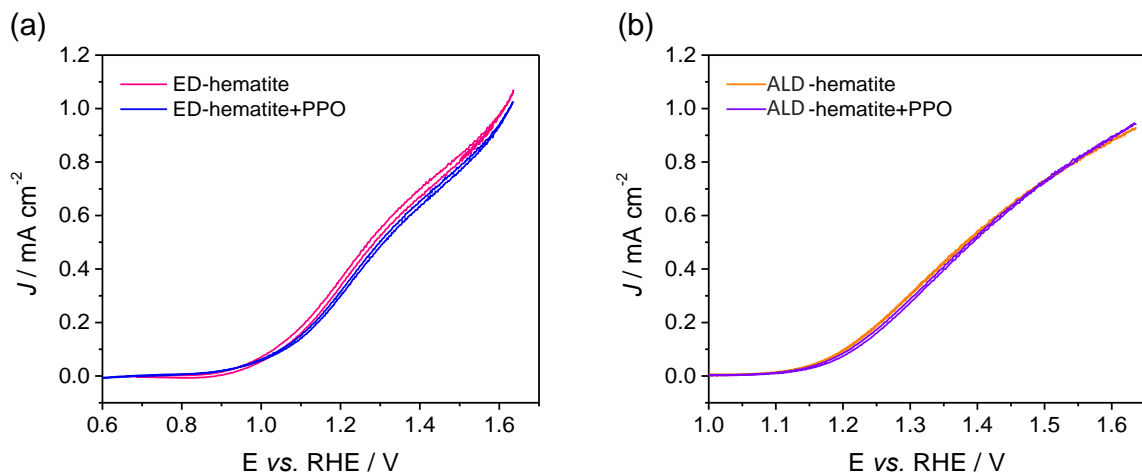
97



98 **Figure S5. Pinhole-free hematite thin film prepared via ALD.** Dark CV response of the bare FTO
 99 (black), ED-hematite (pink) and ALD-hematite (orange) in 1.0 M KOH containing 10 mM $k_4[Fe(CN)_6]$
 100 solution. The scan rates are 10 mVs^{-1} . The negligible current density recorded for the ALD-hematite
 101 compared to the FTO and ED-hematite indicates a pinhole-free hematite thin film achieved.
 102



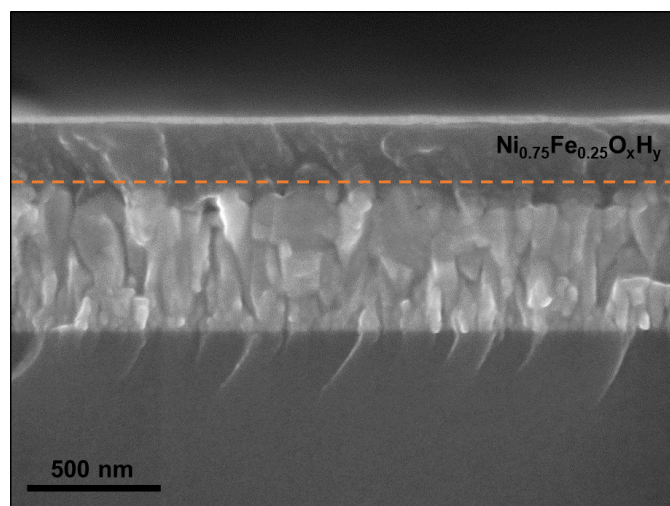
103 **Figure S6. Evidence of selective PPO deposition on FTO.** The measured current density during the first
 104 scan of PPO electrodeposition on different surfaces, including bare FTO (black), ED-hematite (pink) and
 105 ALD-hematite (orange). A negligible current was recorded for pinhole-free ALD-hematite suggests that
 106 hematite surface is electrocatalytically inactive for PPO deposition. Scan rates are 100 mVs^{-1} .



107 **Figure S7. PPO deposition does not compromise the hematite performance for PEC OER.** Comparing
 108 the J - E responses for the a) ED-hematite before (pink) and after deposition of PPO (blue) and b) ALD-
 109 hematite before (orange) and after deposition of PPO (violet). Measurements were executed at a scan rate
 110 of 10 mV s^{-1} under 1 sun illumination in 1.0 M KOH .

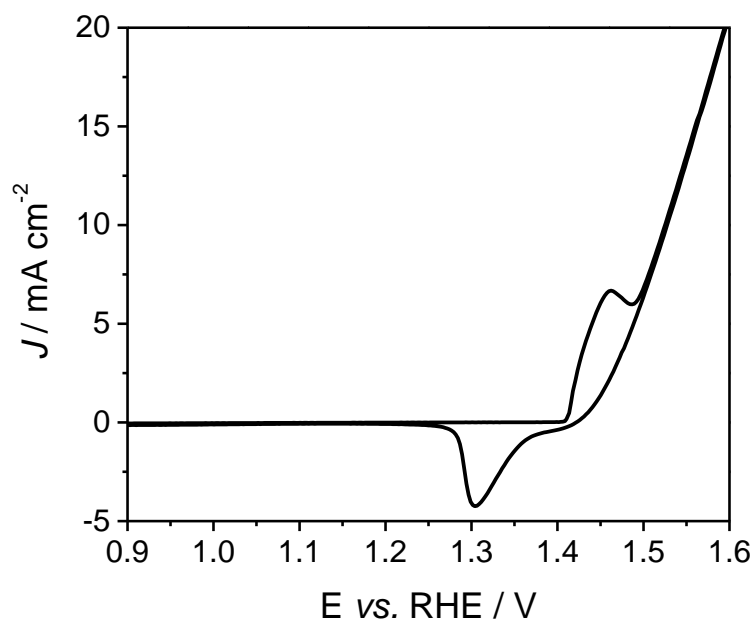
111

112



113

114 **Figure S8. Cross-sectional scanning electron microscopy image of ED-hematite modified with**
 115 **$\text{Ni}_{0.75}\text{Fe}_{0.25}\text{O}_x\text{H}_y$.**



116

117 **Figure S9. *J-E* response of the $\text{Ni}_{0.75}\text{Fe}_{0.25}\text{O}_x\text{H}_y$ electrocatalyst deposited on the FTO substrate.**

118

119 **References:**

- 120 1 O. Zandi, J. A. Beardslee and T. Hamann, *J. Phys. Chem. C*, 2014, **118**, 16494–16503.
- 121 2 O. Zandi, A. R. Schon, H. Hajibabaei and T. W. Hamann, *Chem. Mater.*, 2016, **28**, 765–771.
- 122 3 D. J. Comstock and J. W. Elam, *Chem. Mater.*, 2012, **24**, 4011–4018.
- 123 4 B. A. Gregg, F. Pichot, S. Ferrere and C. L. Fields, *J. Phys. Chem. B*, 2001, **105**, 1422–1429.
- 124 5 R. D. L. Smith, M. S. Prevot, R. D. Fagan, Z. Zhang, P. A. Sedach, M. K. J. Siu, S. Trudel and C.
- 125 P. Berlinguette, *Science (80-.)*, 2013, **340**, 60–63.

126